Computers and Electronics in Agriculture 141 (2017) 171–180

Contents lists available at ScienceDirect

Computers and Electronics in Agriculture

journal homepage: www.elsevier.com/locate/compag

Detection and discrimination of pests and diseases in winter wheat based on spectral indices and kernel discriminant analysis

Yue Shi [a,b,1], Wenjiang Huang [a,*,1], Juhua Luo [c], Linsheng Huang [d], Xianfeng Zhou [a,b]

[a] Key Laboratory of Digital Earth Science, Institute of Remote Sensing and Digital Earth, Chinese Academy of Sciences, Beijing 100094, China
[b] University of Chinese Academy of Sciences, Beijing 100049, China
[c] State Key Laboratory of Lake Science and Environment, Nanjing Institute of Geography and Limnology, Chinese Academy of Science, Nanjing 210008, China
[d] Key Laboratory of Intelligent Computer & Signal Processing, Ministry of Education, Anhui University, Hefei 230039, China

ARTICLE INFO

Article history:
Received 10 March 2017
Received in revised form 24 July 2017
Accepted 25 July 2017

Keywords:
Spectral indices
Kernel discriminant analysis
Automatic detection
Winter wheat
Pests and diseases

ABSTRACT

Kernel discriminant analysis (KDA) can be used as a feasible strategy for identifying plant stresses, especially for detection of pests and diseases, considering the highly nonlinear distribution of hyperspectral absorption features that respond to biophysical variations in plants caused by foliar lesions. However, traditional computation of the kernel projection features produced by hyperspectral data is always affected by redundant information among the numerous wavelengths, subsequently leading to dimension disaster. In order to alleviate this problem, the aim of this study is to propose a spectral vegetation indices-based kernel discriminant approach (SVIKDA) for the detection and classification of yellow rust, aphid, and powdery mildew in winter wheat at the leaf and canopy level. Leaf and canopy level hyperspectral reflectance datasets were measured with a total of 314 and 187 samples, respectively. Fourteen Spectral Vegetation Indices (SVIs) related to foliar biophysical variations were employed as the input sample space; then, by using correlation analysis and independent *t*-tests, redundant information among SVIs was removed. Subsequently, a Gaussian kernel function was utilized to cast discriminant analysis into a nonlinear framework. Finally, using 5-fold cross validation, performance and transferability of this approach were evaluated. Our results revealed that the SVIKDA outperformed conventional linear discriminant approach on detection and classification among healthy wheat leaves and leaves infected with yellow rust, aphids, and powdery mildew. At the leaf level, the classification returned the overall accuracies (OA) of 82.9%, 89.2%, 87.9% for three occurrence levels, i.e. slight, moderate, and severe (Kappa > 0.85). Depending on the types and severities of infestations, the classification accuracy was between 76% and 95%; At the canopy level, the multiple classifications between healthy leaves and leaves with damages from the three different infestations still achieved an accuracy greater than 87% (Kappa = 0.84). In addition, this approach was also successfully applied in disease index (DI) estimation for a specific infestation at the leaf level, and optimal DI estimation returned high coefficients of determination ($R^2 > 0.7$). Furthermore, compared with the commonly used automatic classification algorithm, the SVIKDA achieved an accurate classification without losing the pathological basis of input variables. The results suggest that this method has reliable transferability and great robustness in detecting and discriminating pests and diseases for guiding precision plant protection.

1. Introduction

Global change and natural disturbances have already caused a severe co-epidemic of pests and diseases in winter wheat (*Triticum aestivum L.*), such as aphids, fusarium, yellow rust, and powdery mildew. These threats may result in serious deterioration of grain yield and quality (Savary et al., 2012). Traditionally, manual scouting has been the only way to detect and discriminate these crop pests and diseases (Duveiller et al., 2007), but these investigations are expensive and time-consuming. Even after having identified the distribution of different infected wheat patches, precise use of bactericides and pesticides is hard to achieve in entire fields (Luck et al., 2011; Mahlein et al., 2012). To mitigate the problems of crop monitoring and pesticide overuse, real-time characterization, identification, and classification of different pests and

* Corresponding author.
E-mail addresses: shiyue@radi.ac.cn (Y. Shi), huangwj@radi.ac.cn (W. Huang), jhluo@niglas.ac.cn (J. Luo), zhouxf@radi.ac.cn (X. Zhou).
[1] Yue Shi and Wenjiang Huang contributed equally to this.

http://dx.doi.org/10.1016/j.compag.2017.07.019
0168-1699/

diseases is a necessity. As a non-destructive way of collecting ground information, hyperspectral remotely sensed technologies have proven to be feasible in lesion detection and vitality monitoring (Buitrago et al., 2016; Jaillais et al., 2015; Lópezlópez et al., 2016; Yuan et al., 2013). Among different types of spectral features, spectral vegetation indices (SVIs) are efficient ways to capture the weak spectral signals that indicate certain foliar biophysical variations caused by pests and diseases, such as pigment degradation, reduction in canopy biomass, and a decrease in leaf water content. Huang et al. (2003) determined the sensitive bands of stripe rust at 350 nm, 780 nm, and 1250 nm, and based on these findings, they proposed to use the photochemical reflectance index (PRI) to quantify disease severity at the canopy level. Bravo et al. (2003) used wheat canopy spectral information at the ranges of 740–760 nm and 620–640 nm to calculate the Normalized Difference Vegetation Index (NDVI) and to successfully extract wheat patches with powdery mildew. Feng et al. (2016) measured canopy spectra of wheat at different levels of powdery mildew incidence, suggesting that the best two-band vegetation index ranges for powdery mildew detection were between 570–590 nm and 536–566 nm for the ratio vegetation index (RVI), and 568–592 nm and 528–570 nm for NDVI. These studies have demonstrated that a high spectral resolution, i.e. the use of narrow bands, is essential to discriminate biophysical variations in leaves caused by different infestations, since broadband indices are unable to exploit the subtle spectral features, meanwhile, the use of broadband information would limit the practical use of such approaches to the availability of hyperspectral data (Gamon et al., 1992). Therefore, in this study, only the hyper-spectral vegetation indices are employed.

Practical applications of remote techniques for crop control and management are lacking, and automatic or semi-automatic methods for detecting and monitoring various pests and diseases have been rarely considered, owing to the fact that 1) the pre-existing infestation sensitive indices are nonlinearly varying as the increase of pathogen attack (Bannari et al., 2007), 2) spectral feature diversities among the different pests and diseases are too weak to be discriminated (Guan et al., 2014; Huang et al., 2014). In order to alleviate these problems, nonlinear extensions of statistical learning methods through the "kernel trick" have been proposed to extract the principle components of input samples without losing the key pathogen attack information that allows for the separation of pests and diseases by species and severity (Mika et al., 1999), Then accurate and robust classification results could be achieved with hyperspectral data (Bengio et al., 2004). The main idea of kernel-based approaches is to map input data to a novel feature space through a nonlinear mapping, which produces a set of projective feature vectors by maximizing the between-class covariance and minimizing the within-class covariance (Baudat and Anouar, 2000). These methods integrate statistics and geometry in the so-called "kernel approaches" framework (Van et al., 2002). For instance, Cai et al. (2007) made use of spectral regression and kernel discriminant analysis (KDA) for facial recognition. Its computational costs was lower than the traditional linear discriminant analysis.

However, the computational progress of the projective feature vectors in the pre-existing KDA approaches involves eigen-decomposition of an input matrix, which is very expensive when a large number of hyperspectral bands are put into the model. For better achievement of KDA in quantitative remote sensing spectra processing, adopting sensitive SVIs instead of original hyperspectral reflectance as the initial input matrix may be a potential solution to this problem. In addition, given our literature review, the nonlinear discriminant technique has received little attention for detecting and classifying crop pests and diseases. In our review, using the combinations and transformations of SVIs as the original input sample space to develop a kernel function for KDA progress was still lacking in the field of agricultural quantitative remote sensing. Therefore, to facilitate both comprehensive combination of the sensitive SVIs and efficient computation in KDA, an SVI-based kernel discriminant analysis (SVIKDA) was proposed in this study to identify the healthy wheat and wheat infested with yellow rust, powdery mildew, and aphid by enhancing the between-classes covariance and narrowing the within-class covariance. Fourteen spectral vegetation indices (SVIs) were utilized for characterizing the foliar lesions caused by different pests and diseases. After filtering the redundant information among SVIs, our method effectively achieved the following objectives: 1) detect the spectral features of diseased and non-diseased wheat leaves, 2) differentiate infestations of yellow rust, aphids, and powdery mildew at both leaf and canopy levels, and 3) estimate the severity levels of each infestation. This study will also provide a theoretical basis for applying hyperspectral remote sensing to quantitatively classify and monitor different diseases and pests on wheat from a relatively early stage, and guide accurate field management.

2. Materials and methods

2.1. Experimental design and pathogen inoculation

The experiment was conducted at the Precision Agriculture Experimental Base in Xiaotangshan, Changping, Beijing (40°10.6′N, 116°26.3′E). The makeup of topsoil nutrients (0–30 cm depth) in the experimental area was as follows: soil organic matter 1.41–1.47%, nitrogen 0.07–0.11%, available phosphorus content 20.5–55.8 mg kg^{-1}, and rapidly available potassium 116.6–128.1 mg kg^{-1}.

Two cultivars of winter wheat '98-100' and 'Jingdong8' were selected due to their susceptibility to both yellow rust and powdery mildew. The cultivars '98-100' and 'Jingdong8' were inoculated with yellow rust and powdery mildew, respectively. In accordance with the National Plant Protection Standard (NPPS), yellow rust and powdery mildew were inoculated by spore inoculation in early April. The wheat cultivar 'Jingdong 8' was inoculated with aphids. During the growing season of winter wheat, wheat aphids occurred in the experimental field patches naturally.

2.2. Data acquisition

2.2.1. Spectral measurement of leaf and canopy samples

In this study, an ASD FieldSpec spectrometer (Analytical Spectral Devices, Inc., Boulder, CO, USA) was utilized to collect the leaf and canopy spectral information. The spectrometer was fitted with 25° field-of-view bare fiber-optic cable, and operated in the 350–2500 nm spectral region. The sampling interval was 1.4 nm between 350 and 1050 nm, and 2 nm between 1050 and 2500 nm. The spectral resolution was 3 nm for the region of 350–1000 nm and 10 nm for the region of 1000–2500 nm.

For leaf spectral measurement, the ASD spectrometer was equipped with a Li-Cor 1800-12 integration sphere (Li-Cor, Inc., Lincoln, NE, USA) used to collect the reflectance and transmittance of the upper surfaces of leaves. Considering the similar characters of near infrared bands between 800 and 1000 nm, only 400–800 nm spectral region was used in analysis. For each sampled leaf of wheat, five different zones were used to quantify the small but not negligible within-leaf variability. The scan time required for each sample was about two minutes. The sample was illuminated by a focused beam, and the radiation captured by the spectrometer was the average reflected radiation within the Li-Cor 1800-12 integration sphere. Data were collected around the middle of April, since the three diseases were in the incidence stage at that time. In the present study, spectra of 209 yellow rust-infested leaves, 140 aphid-infested leaves, and 133 powdery mildew-infested

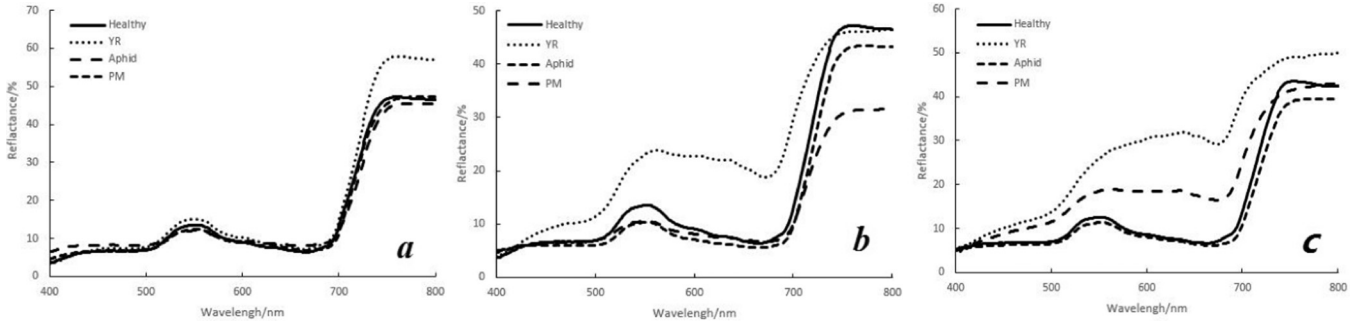

Fig. 1. Average spectral signature of healthy leaves and yellow rust-, aphid- and powdery mildew-infested leaves at three incidence levels: *a* slight: 10% ≤ INL < 40%, *b* moderate: 40% < INL ≤ 70%; *c* serious: 70% < INL ≤ 100%.

leaves were measured. The average spectral curves at different incidence levels (INL) are presented in Fig. 1.

The canopy spectra were taken from a height of 1.3 m above the ground (the height of the wheat was 90 ± 3 cm at maturity). A 40 cm × 40 cm BaSO4 calibration panel was used for reflectance calculation. All irradiance measurements were recorded as an average of 20 scans at an optimized integration time. All measurements were made under clear blue sky conditions between 10:00 and 14:00 (Beijing local time).

2.2.2. Determination of disease severity

The disease index (DI) has been commonly cited to describe the severity of wheat diseases denoted by the portion of disease pustules on the leaf (Graeff and Claupein, 2007). All of the sample leaves were inspected by the National Rules for the Investigation and Forecasting of Crop Diseases (GB/T 15795-1995). Due to the difficulty of accurate assessment, the sample leaves with a lesion coverage ratio less than 1% were regarded as a healthy class. According to this rule, the damaged wheat leaves were grouped into three classes, slight (0% ≤ DI ≤ 20%), moderate (20% < DI ≤ 45%), and severe (DI > 45%). The DI was calculated using Eq. (1)

$$DI(\%) = \frac{\sum(x \times f)}{n \times \sum f} \times 100 \quad (1)$$

where f is the total number of leaves of each degree of disease severity, x is the INL, and n is the highest incidence level.

2.3. Analytical methods

2.3.1. Selection of pre-existing SVIs

The main objective of this step was to find the SVIs sensitive to physiological and biochemical variations caused by yellow rust, aphids, and powdery mildew. Specifically, 14 candidate SVIs were adopted, namely for the biophysical parameters: Normalized Difference Vegetation Index (NDVI), Modified Simple ratio (MSR), Ratio Vegetation Structure Index (RVSI), Health-index (HI); for pigment variation: Structural Independent Pigment Index (SIPI), Normalized Pigment Chlorophyll Index (NPCI), Anthocyanin Reflectance Index (ARI), Modified Chlorophyll Absorption Reflectance index (MCARI); for water and nitrogen content: Nitrogen Ratio Index (NRI), for photosynthetic activity: Photosynthetic Radiation Index (PRI), Physiological Reflectance Index (PHRI); and for crop disease: Yellow rust-index (YRI), aphid index (AI), and Powdery Mildew-index (PMI), The definitions, descriptions, and reference sources for these 14 SVIs are summarized in Table 1.

2.3.2. Pre-processing of the spectral feature sets

In order to create a high-efficiency operation, we reduced the redundant information and multicollinearity effect between the candidate spectral features by making an *a priori* knowledge-based pre-selection to get rid of excessive correlated vegetation indices by using two standards: (1) A correlation analysis (CA) was used between SVIs and DI to screen the SVIs significantly correlated to healthy wheat, yellow rust, powdery mildew, and aphids, (2) An independent *t*-test was used to analyze the response of yellow rust, powdery mildew, and aphids in the SVI set and to screen the specific indices that showed significant heterogeneity to each disease (Daughtry et al., 2000; Gitelson et al., 2001). Finally, intersected SVIs were obtained from the screening sets following these two methods. After this procedure, the selected SVIs not only responded to each disease, but also reflected the significant diversity between them.

2.3.3. Analysis of a nonlinear discriminant algorithm

This work focuses on developing a kernel feature space that can be used to enhance the between-class diversity among the target

Table 1
Spectral vegetation indices and equations used in this study (R = hyperspectral reflectance).

Definition	Equation	Related to	Reference
Modified simple ratio, MSR	$(R_{800}/R_{670}\text{-}1)/(R_{800}/R_{670}+1)^{1/2}$	Leaf area	Chen (1996)
Normalized Difference Vegetation Index, NDVI	$(R_{840}-R_{675})/(R_{840}+R_{675})$	Vegetation coverage	Yuan et al. (2013)
Nitrogen Ratio Index, NRI	$(R_{570}-R_{670})/(R_{570}+R_{670})$	Nitrogen content	Filella et al. (1995)
Photosynthetic Radiation Index, PRI	$(R_{570}-R_{531})/(R_{570}+R_{531})$	Photosynthetic radiation	Gamon et al. (1992)
Structural Independent Pigment Index, SIPI	$(R_{800}-R_{445})/(R_{800}-R_{680})$	Pigment content	Penuelas et al. (1994)
Physiological Reflectance Index, PhRI	$(R_{550}-R_{531})/(R_{550}+R_{531})$	Light use efficiency	Gamon et al. (1992)
Normalized Pigment Chlorophyll Index, NPCI	$(R_{680}-R_{430})/(R_{680}+R_{430})$	Chlorophyll ratio	Penuelas et al. (1994)
Anthocyanin Reflectance Index, ARI	$(R_{550})^{-1}-(R_{700})^{-1}$	Anthocyanin content	Gitelson et al. (2001)
Ratio Vegetation Structure Index, RVSI	$[(R_{712}+R_{752})/2]-R_{732}$	Biomass	Merton (2007)
Modified Chlorophyll Absorption Reflectance index, MCARI	$(R_{701}-R_{671})-0.2(R_{701-549})]/(R_{701}/R_{671})$	Chlorophyll absorption	Daughtry et al. (2000)
Health-index, HI	$(R_{739}-R_{402})/(R_{739}+R_{402})-0.5R_{403}$	Greenness, biomass	Huang et al. (2014)
Yellow rust index, YRI	$(R_{515}-R_{698})/(R_{515}+R_{698})-0.5R_{738}$	Wheat disease	
Aphid-index, AI	$(R_{730}-R_{419})/(R7_{30}+R_{419})-0.5R_{736}$	Wheat pest	
Powdery mildew index, PMI	$(R_{400}-R_{735})/(R_{400}+R_{735})-0.5R_{403}$	Wheat disease	

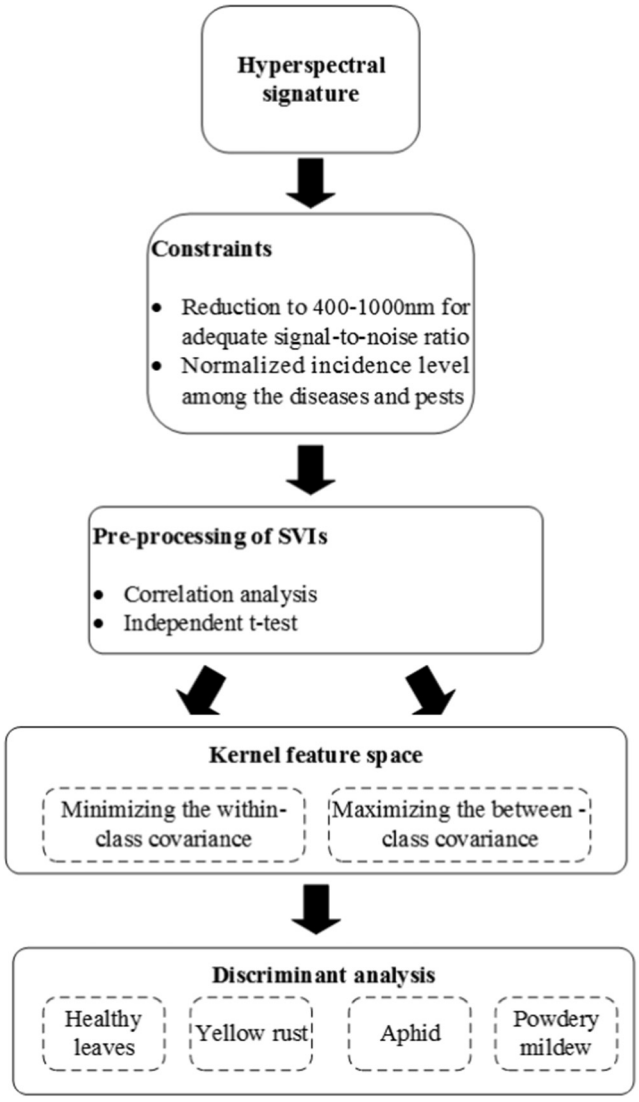

Fig. 2. Systematic approach to develop nonlinear discriminant analysis for pest and disease discrimination.

diseases and pests. Fig. 2 summarizes basic steps from spectral signatures to kernel feature space and then to final classification, which included selecting spectral features, and developing mapping rules.

The fundamental purpose of the nonlinear discriminant analysis is to solve the limitation of linear discriminant analysis, by producing a set of nonlinear discriminant vectors in original space. Mathematically, for a given mapping rule Φ, the pattern in the original input data space R^n could be mapped in to a new feature space F

$$\Phi : SVIs \mapsto R^n \tag{2}$$

$$x \mapsto \Phi(x) \tag{3}$$

The nonlinear discriminant can be achieved by maximizing the following criterion:

$$J^K(\alpha) = \frac{\alpha^T (KWK)\alpha}{\alpha^T (KK)\alpha} \tag{4}$$

where the matrix K is the kernel function matrix corresponding to a given nonlinear mapping Φ, and W = diag(W_1, W_2,. . .,W_c), where W_j (j=1,2,. . .,c) is a training samples matrix of class i. The details of these definitions can be found in a study by Yang et al. (2004).

For solving this optimization problem, we considered the decomposition of matrix K (Theodoridis and Koutroumbas, 2010). Supposing that $\gamma_1, \gamma_2, \ldots, \gamma_m$ are K's orthonormal eigenvectors corresponding to m (m is the rank of K) nonzero eigenvalues $\lambda_1 \geqslant \lambda_2 \geqslant \ldots \geqslant \lambda_m$, K can therefore be represented by

$$K = P\Lambda P^T \tag{5}$$

where $P = (\gamma_1, \gamma_1, \ldots, \gamma_m)$, and $\Lambda = diag(\lambda_1, \lambda_2, \ldots, \lambda_m)$

Substituting Eq. (5) onto Eq. (4) and defining β as:

$$\beta = \Lambda^{\frac{1}{2}} P^T \alpha \tag{6}$$

then Eq. (4) could be simplified into

$$J^K(\beta) = \frac{\beta^T (S_b)\beta}{\beta^T (S_t)\beta} \tag{7}$$

where

$$S_b = \Lambda^{\frac{1}{2}} P^T W P \Lambda^{\frac{1}{2}} \tag{8}$$

$$S_t = \Lambda \tag{9}$$

It is obvious that S_t is positive definite and S_b is semi-positive definite. Therefore, Eq. (7) is a regular generalized Rayleigh quotient. By maximizing this equation, we can obtain a set of optimal solutions $\beta_1, \beta_2, \ldots, \beta_d$, which were the largest eigenvalues of $S_t^{-1} S_b$. Subsequently, it is easy to obtain a set of optimal solutions α_j (j = 1, 2, . . ., d) from Eq. (6). Therefore, the optimal canonical discriminant score φ_j in features space is:

$$\varphi_j = Q\alpha = QP\Lambda^{-\frac{1}{2}}\beta \tag{10}$$

2.3.4. Calibration and validation of models

In order to assess the efficiency of the nonlinear discriminate algorithm, we employed Jeffreys-Matusita Distance (JM-distance) as the standard to quantify the separability between the different classes (Kailath, 1967). The JM-distance threshold was set as 1.8 in this study.

Generally, training data and testing data have to be separated to assess the SVIKDA model. To achieve a sufficient utilization of all information in the training data, the classification performance was evaluated by cross-validation, thus, the entire data set was divided into k mutually exclusive groups following a k-fold cross-validation partitioning design, out of which k-1 were used for training, and the remaining used for validation (Kohavi, 1995). Meanwhile, the Kappa value and Confusion Matrix, were used as two important performance indicators for classification. These accuracy indicators were given by the average values (Saadi et al., 2007).

For each species of pests and diseases, the canonical discriminant scores were used to build the calibration models, thus, the regression equations were then inverted to estimate the DIs of the testing data set. Here, three types of regression models (*linear*, *exponential*, and *polynomial*) built with k-folds partitions were employed. Note that each estimation model allowed us to compare between the estimated DIs and measured DIs, and evaluate the performance of the canonical discriminant scores on DIs prediction. These methods reduced the dependence on a single partition into validation data sets. It also guaranteed that all samples were used for both training and validation with each sample used for validation exactly once. The coefficient of determination (R^2) and root mean square error (RMSE) were employed as the accuracy indicators.

3. Results

3.1. Sensitive SVIs for yellow rust, aphids, and powdery mildew

The threshold-based classification ability tests of each SVI for different diseases and pests are shown in Table 2. Meanwhile, the correlation analyses and the independent *t*-tests of the SVIs are shown in Table 3. The intersection of these SVIs represents the ideal features that contributed most in differentiating among the healthy class and pest and disease classes, including MSR, PRI, SIPI, HI, YRI, and PMI.

3.2. Classification and prediction of healthy leaves and leaves with symptoms of yellow rust, aphids, and powdery mildew

The SVIs identified by the correlative analysis and independent *t*-test were used as the input sample space to train the SVIKDA. Following the procedure of Section 2.3.3, we selected a Gaussian Kernel for nonlinear mapping of feature space:

$$k(x,y) = \exp\left(-\frac{\|x-y\|^2}{2\sigma^2}\right), \quad \sigma \in R \tag{11}$$

Table 2
Comparison of the independent classification abilities of the candidate SVIs.

Vegetation indices	Classification accuracy (%)			
	Healthy	Yellow rust	Aphids	Powdery mildew
MSR	***	*	*	*
NDVI	**	**	*	**
NRI	*	*	*	*
PRI	*	***	*	**
SIPI	*	**	*	***
PhRI	*	**	*	*
NPCI	*	**	*	**
ARI	*	**	*	**
AVSI	*	**	*	*
MCARI	*	*	*	*
HI	***	**	**	**
YRI	**	***	**	**
AI	**	*	***	**
PMI	*	**	***	***

Note:
*** Classification accuracy ≥ 60%.
** 30% ≤ classification accuracy < 60%.
* Classification accuracy < 30%.

Table 3
Correlative analysis and independent *t*-test of different SVIs.

	Correlation				Independent *t*-test			
	H	YR	A	PM	H&Oth	YR&Oth	A&Oth	PM&oth
MSR	+				+			
NDVI	+		+	+				
NRI								
PRI		+		+		+		
SIPI				+				
PhRI								
NPCI								
ARI		+		+				
AVSI								
MCARI								
HI	+				+			
YRI		+				+		
AI			+					
PMI			+	+			+	+

Note: + significant spectral vegetation indices (for correlation analysis, $p < 0.05$; for independent *t*-test, $p < 0.05$). H = healthy, YR = yellow rust, A = aphid, PM = powdery mildew, Oth = Others.

In this case, to better test the classification ability at the three different occurrence levels, three classification models were established, i.e. slight, moderate, and severe, respectively. Here, the canonical discriminant coefficients are listed in Table 4, which illustrates that MSR, SIPI, and PMI dominated the first canonical discriminant function ($R^2 > 0.7$) (CDF-1); PRI and SIPI dominated the second canonical discriminant function (CDF-2); while HI and YRI dominated the third canonical discriminant function (CDF-3).

For the slight level, CDF-1 significantly accounted for 59.1% of the variation, and CDF-2 accounted for 28%, i.e. the accumulated contribution reached 87.1%; for the moderate level, CDF-1 significantly accounted for 67.1% of the variation, and CDF-2 also accounted for 30.8% (i.e. the accumulated contribution reached 94.9%); for the severe level, the CDF-1 significantly accounted for 74.2%, while CDF-2 only accounted for 21.3% (i.e. the accumulated contribution reached 95.5%). The first two canonical discriminant functions were employed to establish the projective scatter of discriminate scores (Fig. 3). It was clear that, for the slightly diseased level, CDF-1 was able to discriminate the aphid-infected leaves from other classes, but, with the addition of CDF-2, the between-class distances among classes were magnified (JM distance greater than 1.8) (Fig. 3a). For the moderate level, CDF-1 revealed great performance for detection of all infestation samples, while CDF-2 was able to discriminate the healthy samples (JM distance greater than 1.9) (Fig. 3b). Similarly, for the severe level, the combination of CDF-1 and CDF-2 performed better for differentiating diversities among healthy and infestation classes (JM distance greater than 1.8).

The Confusion Matrix for classification based on the cross-validation samples is shown in Table 5, which clearly demonstrates that the overall accuracies at the three DI levels were, respectively, 82.9%, 89.2%, 87.9%, and the Kappa values at the three occurrence levels were greater than 0.8. For the slight level, the highest misclassification existed in the aphid-infested samples; for moderate and severe levels, the main misclassification occurred between yellow rust- and powdery mildew-infested samples.

Based on the discriminant scores calculated by CDF-1, the empirical regression models were determined, and the resultant predictive equations are listed in Table 6. The results demonstrated that, for the slight occurrence level, the relationship between the DIs and the scores were exponential, with the optimal values of R^2 greater than the linear and polynomial models; while for moderate and severe levels, the linear regression outperformed the other two models in DI prediction.

The scatter plots between the measured DIs and the estimated DIs are illustrated in Fig. 4. The reliability of the regression equation was satisfactory, with R^2 values of 0.78, 0.82, and 0.83, and RMSE values of 2.79, 2.02, and 2.3 for the three targeted pests and diseases at the slight occurrence level (Fig. 4a–c); R^2 values of 0.86, 0.79, and 0.85, and RMSE values of 2.4, 3.47, and 2.28 at the moderate occurrence level (Fig. 4d–f); and R^2 values of 0.88, 0.89, and 0.79, and RMSE of 4.49, 3.34, and 3.58 at the severe occurrence level (Fig. 4g–i), indicating that it is feasible to use the canonical discriminant scores to build prediction models for estimating the severities of pests and diseases with yellow rust, aphids, and powdery mildew.

3.3. Accuracy assessment of KDA

Based on the 5-fold cross validation datasets, the accuracy indices returned by the best and worst classifications are listed in Table 7. Meanwhile, for the validation of the DI prediction model, a comparison of the best and worst convergence based on the optimal prediction models is shown in Fig. 5. These results illustrate that, for the proposed KDA approach, the accuracies for both classification and DI estimations only varied in a limited range for different DI levels. In addition, from a small sample

Table 4
Standardized canonical coefficients (SCCs) and correlation coefficients (CCs) of discriminant canonical functions developed by the identified SVIs.

SVIs	SCCs			CCs		
Slight	CDF-1	CDF-2	CDF-3	CDF-1	CDF-2	CDF-3
MSR	0.354	−3.677	2.526	0.960	0.181	−0.045
PRI	−1.220	2.802	1.104	−0.171	0.457	0.444
SIPI	3.382	2.511	1.095	0.620	−0.695	0.0561
HI	−3.336	−3.092	−14.558	0.179	−0.237	−0.801
YRI	−1.073	−3.271	1.491	−0.107	0.122	0.612
PMI	2.620	−1.896	0.889	0.575	0.158	0.174
Moderate						
MSR	0.072	−0.747	0.513	−0.766	0.053	0.395
PRI	−0.314	0.722	0.285	0.309	0.653	−0.294
SIPI	0.845	0.627	0.274	0.543	−0.616	−0.407
HI	−0.171	−0.159	−0.747	0.183	−0.154	0.660
YRI	0.179	−0.695	0.561	0.192	0.114	0.515
PMI	0.220	−0.237	−0.801*	0.472	0.168	−0.174
Severe						
MSR	−1.267	−4.507	−0.273	0.881	0.093	−0.163
PRI	5.665	3.951	−2.559	−0.223	−0.612	0.098
SIPI	−4.764	2.841	−2.345	−0.514	0.576	−0.341
HI	2.360	4.480	10.720	0.058	0.322	0.798
YRI	2.431	−1.216	1.860	0.125	−0.109	0.493
PMI	−2.763	−1.738	−0.107	−0.557	−0.153	−0.183

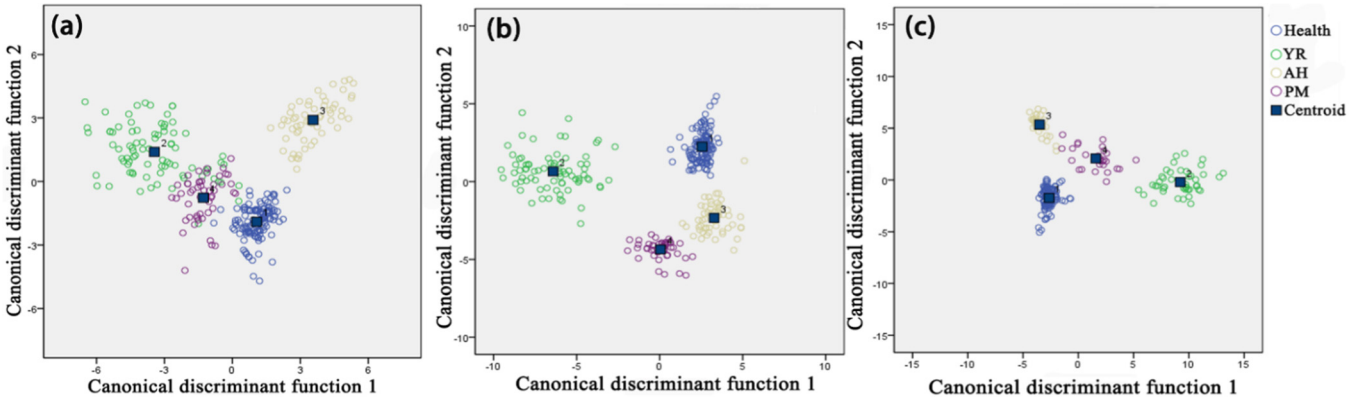

Fig. 3. Projection of the discriminant scores of healthy leaf samples and leaves infected with yellow rust (YR), aphid (AH), and powdery mildew (PM) at (a) slight, (b) moderate and (c) severe occurrence levels.

Table 5
Confusion matrix and accuracy assessment of the SVIKDA for leaf samples.

Prediction		Ground truth				U (%)	OA (%)	Kappa
		Healthy	YR	Aphid	PM			
Slight $0\% \leq DI \leq 20\%$	Healthy	125	5	12	3	86.2	82.9	0.81
	YR	2	71	8	7	79.8		
	Aphid	4	1	48	4	84.2		
	PM	3	6	4	42	76.3		
	P(%)	93.3	85.5	66.7	75			
Moderate $20\% < DI \leq 45\%$	Healthy	130	3	10	2	89.6	89.2	0.87
	YR	2	69	3	2	90.8		
	Aphid	2	1	46	4	86.8		
	PM	1	4	1	44	88		
	P(%)	96.3	89.6	76.7	84.6			
Severe $DI > 45\%$	Healthy	138	2	4	1	95.2	87.9	0.83
	YR	2	36	1	5	81.8		
	Aphid	2	0	24	1	88.9		
	PM	1	2	1	21	84		
	P(%)	97.2	90	80	75			

Notes: OA = overall accuracy, P = producer's accuracy, U = user's accuracy.

training perspective, different populations of training samples were tested to observe the performance of the variables to evaluate the scaling impact on the estimated DI, According to Fig. 5, the coefficient of determination R^2 at different scales increased in a similar logarithmic function. It was clear that the rate of convergence of R^2 was consistent, when the average training population was greater than 40, R^2 would be greater than 0.8.

3.4. Validation and application at the canopy scale

To further validate the transferability of this nonlinear discriminant approach, independent in-field canopy spectral data of yellow rust, aphids, and powdery mildew were used. Owing to the lack of a healthy wheat field during the sample period, only the infestation samples were utilized. Considering that the accumulated contribution rate of the CDFs was not as significant as the leaf level (i.e., the first three CDFs accounted for 49.5%, 27% and 15.2%, respectively), here, we employed the first three CDFs to build the projective space. The scatter plots of the discriminant scores and the classification results are shown in Fig. 6 and Table 8, respectively. For these non-imaging canopy data, the JM-distances among different classes were greater than 1.8, the producer's accuracies for yellow rust-, aphid- and powdery mildew-infested wheat were 88.2%, 91.8% and 87.9%, and the user's accuracies were 89.1%,

Table 6
Statistical analysis of the relationship between canonical discriminant scores (x) and the predicted DI (y) of each pest and disease.

	Slight		Moderate		Severe	
	Prediction equation	R^2	Prediction equation	R^2	Prediction equation	R^2
YR	$y = 0.9338x + 0.6796$	0.695	$y = 0.966x + 0.6571$	0.681	$y = 0.9338x + 5.002$	0.689
	$y = 1.732e^{0.75x}$	0.726	$y = 0.4104e^{0.344x} + 0.145$	0.559	$y = 1.4087e^{0.707x} + 0.0148$	0.672
	$y = -0.0382x^2 + 0.2337x + 0.5024$	0.701	$y = -0.1057x^2 + 1.2548x + 1.0134$	0.492	$y = 0.4119x^2 + 1.2548x + 1.0134$	0.615
AH	$y = 0.8111x + 1.5573$	0.612	$y = 1.0213x - 1.6314$	0.675	$y = 0.9531x + 1.1606$	0.655
	$y = 0.21e^{0.49x}$	0.719	$y = 0.9843e^{0.4373x}$	0.657	$y = 0.6883e^{0.6379x} + 1.1587$	0.534
	$y = -0.0291x^2 + 0.2308x + 0.3043$	0.704	$y = -0.016x^2 + 0.1572x + 0.1042$	0.440	$y = -0.0089x^2 + 0.1169x + 0.1471$	0.537
PM	$y = 0.9495x + 4.447$	0.696	$y = 0.9531x + 1.1606$	0.728	$y = 0.8738x - 10.6368$	0.710
	$y = -0.0323e^{0.22x} + 0.0131$	0.721	$y = 0.0052e^{0.552x} - 0.0166$	0.624	$y = -0.0114e^{0.1755x} + 0.0727$	0.641
	$y = -0.0287x^2 + 0.2423x + 0.1129$	0.696	$y = -0.0004x^2 + 0.0042x + 0.0017$	0.677	$y = -0.01x^2 + 0.1267x + 0.1223$	0.545

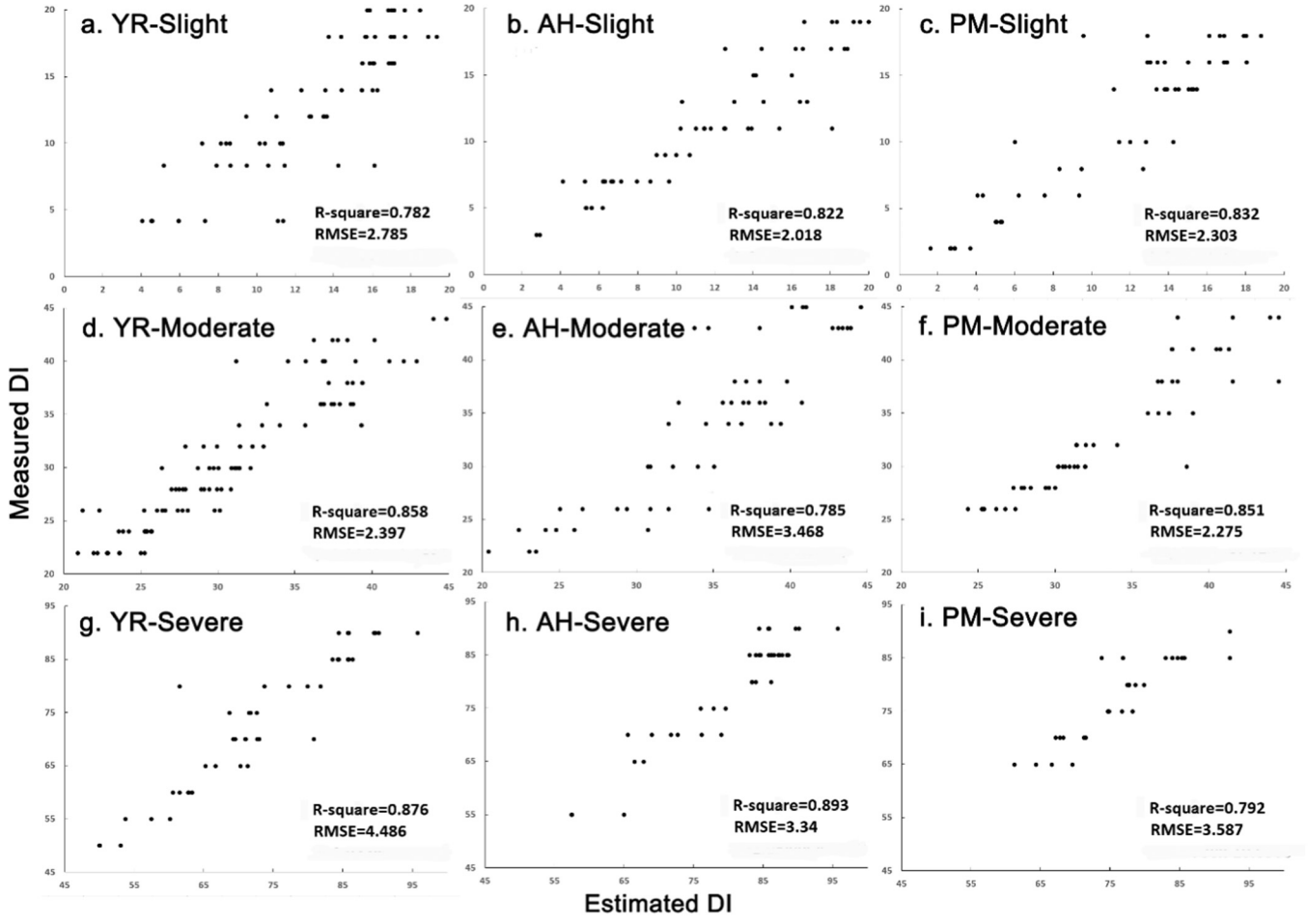

Fig. 4. Scatter plots between the measured DIs and the best estimated DIs by SVIKDA at different leaf infestation levels: (a–c) slight occurrence ($0\% \leq DI \leq 20\%$), (d–f) moderate occurrence level ($20\% < DI \leq 45\%$), (g–i) severe occurrence ($DI > 45\%$). Here, YR = yellow rust, AH = aphids, PM = Powdery mildew.

Table 7
Comparison of the classification ability of the SVM classifier with Characteristic Enhancement Space and traditional SVM based on common vegetation indices (SVIs) characteristic space.

Disease severity	Classification state	Classification accuracy (%)			Recall accuracy (%)		
		YR	A	PM	YR	A	PM
0% ≤ DI < 20%	Optimal	79.8	84.2	76.3	85.5	72.7	75
	Worst	67.1	61.3	63.1	81.2	63.4	70.2
20% ≤ DI < 45%	Optimal	90.8	86.8	88	89.6	76.7	84.6
	Worst	83.3	64.7	76.8	83.5	67.5	79.2
DI ≥ 45%	Optimal	89.4	88.9	86	90.8	80	85.4
	Worst	82.1	80.8	84.9	83.3	68.2	83.5

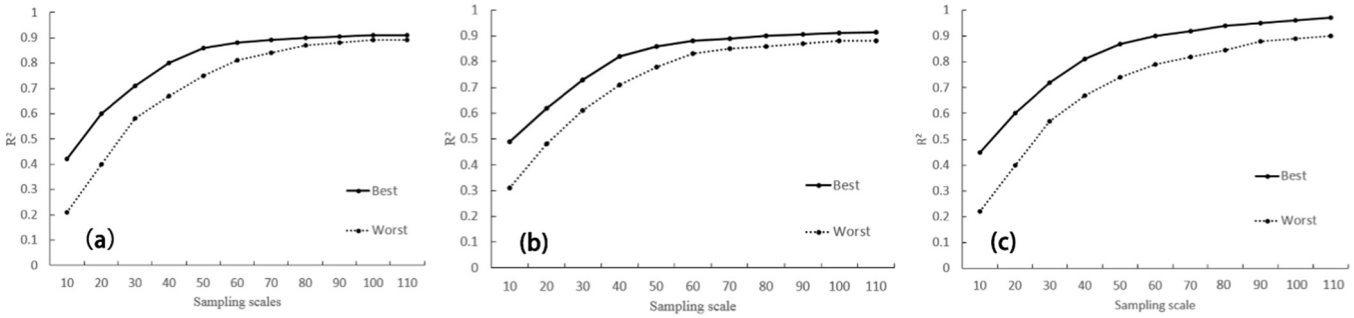

Fig. 5. Comparison of R^2 of estimated DIs on leaf scales with different sample populations. (a) yellow rust, (b) aphids, and (c) powdery mildew.

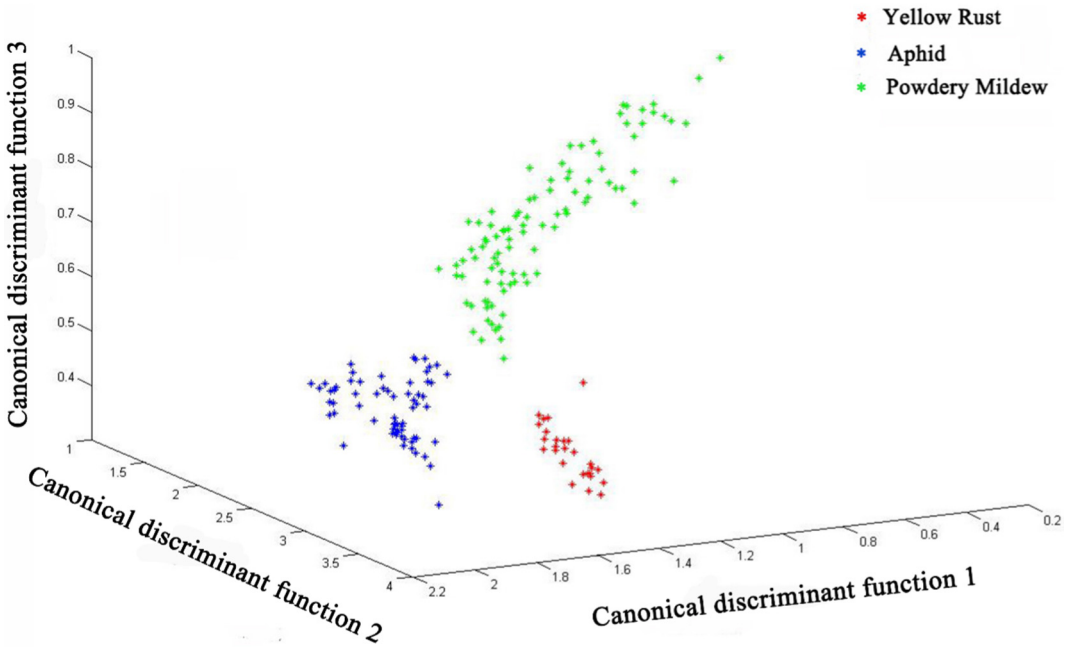

Fig. 6. Scatter plots of the projected positions based on the first three CDFs in the kernel projective space.

Table 8
Confusion matrix and accuracy assessment of SVIKDA for canopy samples.

Prediction	Ground truth			U/%	OA/%	Kappa
	YR	Aphid	PM			
YR	57	1	6	89.1	87.7	0.84
Aphid	3	23	6	74.2		
PM	5	2	84	92.3		
P/%	88.2	91.8	87.9			

Notes: OA = overall accuracy, P = producer's accuracy, U = user's accuracy.

74.2%, and 92.3%, respectively. Meanwhile, the main misclassification emerged between yellow rust and powdery mildew, which was similar to the results at the leaf level.

4. Discussion

In general, the foliar symptoms caused by yellow rust, aphids, or powdery mildew could induce wilting and discoloration in appearance, and result in a series of physiological and biochemical variations of leaves, i.e. pigments, internal and external structure, water content, and biochemical concentration, subsequently impacting photosynthetic activity (Goward et al., 2002; Moshou et al., 2004). These infestation characteristics lead to leaf spectral absorption changes on a series of hyperspectral bands. However, owing to the complexity of the hyperspectral data, SVIs that contain a combination of two or three specific wavelengths were developed to reduce the number of bands (Mirik et al., 2012). In

this study, by using correlation analysis and independent *t*-test, several relevant SVIs were identified, SIPI for pigment variations, PRI for photosynthetic activity, MSR for foliar structure, and HI for plant stresses, YRI and PMI for crop infestations. These SVIs were set as the input feature space for substitution of the original hyperspectral bands in order to reduce effects of the redundancy information and so-called "Hughes Phenomenon" (Pal and Foody, 2010).

Given our literature review, although the SVIs could be regarded as the proxies to deduce biophysical changes in diseased leaves, the detection and discrimination of various pests and diseases based on a single SVI has not been feasible so far. Therefore, a combined use of these comprehensive SVIs enhanced the information content for automatic detection and classification that were tied to the host-pathogen interaction of infestations and the resistance reactions of plant tissues comprehensively, especially in early infected stage when pathogens do not have an advanced attack,. Taking powdery mildew for example, the major symptoms are fluffy white mycelia covering the leaf surface, germs damaging the plant's internal structure and biochemical concentration, subsequently influencing the maximum absorption of carotenoids, causing reflectance changes near 515 nm, 698 nm and 738 nm. These influences of fungal tissue on the leaf surface could be detected by the combination of MSR, PRI, SIPI, and PMI (Penuelas et al., 1995).

This study proved the feasibility of the nonlinear strategy of SVIKDA for detecting and classifying winter wheat leaves inoculated with different infestations. Compared to the conventional linear discriminant analysis (LDA) and support vector machine (SVM) methods, this study took advantage of a kernel mapping function to establish the nonlinear framework of SVIKDA without losing the original biophysical and pathological basis of the input variates. The principle advantage of this is that, based on a minimum squared error cost function, the classification hyperplanes could be obtained without the need for an additional transformation or classification technique. The SVIKDA successfully achieved accurate classification and prediction of yellow rust, aphid, and powdery mildew by adopting the Gaussian kernel function to enhance the between-class variance and minimize the within-class variance, which outperformed the conventional LDA and SVM on the detection of the target pest and diseases. The comparison of average classification error by using LDA, SVM, and SVIKDA is presented in Table 9, which revealed that, by using the same SVIs as the input samples, the SVIKDA classification error for each infestation is noticeably less.

Specifically, as illustrated by the results mentioned in the last section, this nonlinear strategy of SVIKDA was able to improve the detection and discrimination of pests and diseases in several aspects. Firstly, by using the SVIKDA, CDF-1 was regarded as the principle contributor to the detection of healthy wheat leaves from the inoculated leaves, and when combined with CDF-2 or CDF-3, the different species and severities of target pest and diseases were differentiated accurately. Secondly, the 5-folds cross validation indicated that this algorithm returned a relatively stable precision for both classification and DI estimation by using the discriminant scores produced by CDFs. The slight fluctuations could be accounted for the random selection of training data and testing data. The correlated relationship between the measured DIs and the estimated DIs for the slight level was exponential, while for moderate and severe levels, the correlations were closer to linear. Moreover, after testing the effects of a small size of training data, we could conclude that this algorithm has great potential for breaking through the restrictions of small-sample learning, which guaranteed a stable output with precise classification. Finally, this SVIKDA has successfully been utilized at the canopy level, which demonstrates the feasibility and transferability of this method for practical application. In addition, it is noteworthy that, several characteristics of the SVIKDA, such as the mutually complementary of the two discriminant subspaces produced by SVIKDA procedure and its ability to remove the background spectral variation, maybe valuable for disease monitoring with aerial or satellite remote sensing imagery and detecting disease infestations from other stresses (e.g. fertilizer and water stresses) at the regional level. However, the hyperspectral curve measured by a non-imaging sensor is the average reflectance of healthy and diseased leaf tissue (Mahlein et al., 2012). This typically leads to degenerated accuracy for the classification of the characteristic symptoms at the slight occurrence level due to the small destructive colonies. Therefore, considering the diseased tissue on the leaf surface impacts the spectral signatures like a dusty coat (Rumpf et al., 2010), further investigation with imaging sensor system may be necessary for better understanding the pathogen-host interactions and further improving the classification accuracy.

In conclusion, the proposed SVIKDA is characterized by a high sensitivity and robustness for the detection and classification of winter wheat pests and diseases. By implementing this method, a promoted classification accuracy has been achieved. In addition, the ability of this model to be generalized has been proved by a cross-validation procedure. Compared with commonly used linear classification techniques, this progress with SVIKDA provided three obvious improvements in recognizing and discriminating different pests and diseases: 1) synchronism, 2) precision, and 3) efficiency. Furthermore, this procedure even suitable for "high-dimensionality" problem (in observation space), because our findings are more decided by the explicitly pathological foundation of the specific disease and by the "kernel" mapping strategy that turns the high-dimensional original observation into low-dimensional feature subspaces However, further investigation about the interactions of each infestation maybe necessary to explain the difficulties in early detection of characteristic symptoms and further improve the classification accuracy of this model. On the other hand, it can be anticipated that robust hyperspectral imaging sensors based on the pixel-wise attribution of destructive tissue may provide better circumstances for practical use.

Table 9
Comparison of the classification error based on the SVIKDA and conventional LDA.

Leaf state	Classification error (%)		
	SVIKDA	LDA	SVM
Health	3.7	8.9	5.2
Yellow rust	10.4	14.5	12.4
Aphid	16.3	23.5	18.7
Powdery mildew	15.4	20.4	17.5

5. Conclusion

In this study, our results showed that the proposed SVIKDA algorithm has successfully been applied to detecting and identifying the dynamic development of yellow rust, aphids, and powdery mildew at different stages. This approach linked hyperspectral data at the leaf and canopy levels with ground measured winter wheat infestation information. It performed well at three typical occurrence levels of diseases and pests. Three advantages of this method were proved over traditional hyperspectral analysis procedures for detecting pest and disease: 1) it reduced the redundancy information among numerous bands by extracting the most sensitive SVIs for different infestations. 2) it required fewer samples for training and calculating, and 3) it had a flexible framework with modifiable characteristic SVIs. These advantages supported the potential of

this method to be used in other plant- pathogen systems, and facilitated the early detection and identification of pests and diseases at the leaf- and canopy- level or larger scales.

Acknowledgements

This work was supported by the external cooperation program of BIC, Chinese Academy of Sciences (131211KYSB20150034) – China, the National Natural Science Foundation of China (61661136004) – China, and the Open Research Fund of the Key Laboratory of Digital Earth Science, Institute of Remote Sensing and Digital Earth, Chinese Academy of Sciences (2015LDE010) – China, the authors are grateful to Dr. Luke for her editing to the manuscript and to the reviewers for their helpful comments and suggestions.

References

Bannari, A., Khurshidt, K.S., Staenz, K., Schwarz, J.W., 2007. A comparison of hyperspectral chlorophyll indices for wheat crop chlorophyll content estimation using laboratory reflectance measurements. Geosci. Remote Sens. IEEE Trans. 45, 3063–3074.

Baudat, G., Anouar, F., 2000. Generalized discriminant analysis using a kernel approach. Neural Comput. 12, 2385.

Bengio, Y., Delalleau, O., Le, R.N., Paiement, J.F., Vincent, P., Ouimet, M., 2004. Learning eigenfunctions links spectral embedding and kernel PCA. Neural Comput. 16, 2197–2219.

Bravo, C., Moshou, D., West, J., Mccartney, A., Ramon, H., 2003. Early disease detection in wheat fields using spectral reflectance. Biosyst. Eng. 84, 137–145.

Buitrago, M.F., Groen, T.A., Hecker, C.A., Skidmore, A.K., 2016. Changes in thermal infrared spectra of plants caused by temperature and water stress. Isprs J. Photogrammetry Remote Sens. 111, 22–31.

Cai, D., He, X., Han, J., 2007. Efficient Kernel discriminant analysis via spectral regression. IEEE Int. Conf. Data Mining, 427–432.

Chen, J.M., 1996. Evaluation of vegetation indices and a modified simple ratio for boreal applications. Can. J. Remote. Sens. 22, 229–242.

Daughtry, C.S.T., Walthall, C.L., Kim, M.S., Colstoun, E.B.D., Iii, M.M., 2000. Estimating corn leaf chlorophyll concentration from leaf and canopy reflectance. Remote Sens. Environ. 74, 229–239.

Duveiller, E., Singh, R.P., Nicol, J.M., 2007. The challenges of maintaining wheat productivity: pests, diseases, and potential epidemics. Euphytica 157, 417–430.

Feng, W., Shen, W., He, L., Duan, J., Guo, B., Li, Y., Wang, C., Guo, T., 2016. Improved remote sensing detection of wheat powdery mildew using dual-green vegetation indices. Precision Agric. 17, 608–627.

Filella, I., Serrano, L., Serra, J., Penuelas, J., 1995. Evaluating wheat nitrogen status with canopy reflectance indices and discriminant analysis. Crop Sci. 35, 1400–1405.

Gamon, J., Penuelas, J., Field, C., 1992. A narrow-waveband spectral index that tracks diurnal changes in photosynthetic efficiency. Remote Sens. Environ. 41, 35–44.

Gitelson, A.A., Merzlyak, M.N., Chivkunova, O.B., 2001. Optical properties and nondestructive estimation of anthocyanin content in plant leaves. Photochem. Photobiol. 74, 38.

Goward, S.N., Xue, Y., Czajkowski, K.P., 2002. Evaluating land surface moisture conditions from the remotely sensed temperature/vegetation index measurements: An exploration with the simplified simple biosphere model. Remote Sens. Environ. 79, 225–242.

Graeff, S., Claupein, W., 2007. Identification and discrimination of water stress in wheat leaves (Triticum aestivum L.) by means of reflectance measurements. Irrig. Sci. 26, 61–70.

Guan, Q., Huang, W., Zhao, J., Liu, L., Liang, D., Huang, L., Wang, L., Yang, G., 2014. Quantitative Identification of Yellow Rust, Powdery Mildew and Fertilizer-Water Stress in Winter Wheat Using In-Situ Hyperspectral Data. Sensor Lett. 12, 876–882(877).

Huang, M., Wang, J., Huang, W., Huang, Y., Zhao, C., Wan, A., 2003. Hyperspectral character of stripe rust on winter wheat and monitoring by remote sensing. Trans. Chin. Soc. Agric. Eng. 19, 1519–1531.

Huang, W., Guan, Q., Luo, J., Zhang, J., 2014. New optimized spectral indices for identifying and monitoring winter wheat diseases. IEEE J. Selected Topics Appl. Earth Observations Remote Sens. 7, 2516–2524.

Jaillais, B., Roumet, P., Pinson-Gadais, L., Bertrand, D., 2015. Detection of Fusarium head blight contamination in wheat kernels by multivariate imaging. Food Control 54, 250–258.

Kailath, T., 1967. The divergence and Bhattacharyya distance measures in signal selection. Commun. Technol. IEEE Trans. 15, 52–60.

Kohavi, R., 1995. A study of cross-validation and bootstrap for accuracy estimation and model selection. Int. Joint Conf. Artificial Intelligence, 1137–1143.

Lópezlópez, M., Calderón, R., Gonzálezdugo, V., Zarcotejada, P., Fereres, E., 2016. Early detection and quantification of almond red leaf blotch using high-resolution hyperspectral and thermal imagery. Remote Sens. 8, 276.

Luck, J., Spackman, M., Freeman, A., Tre, P., Db, X., bicki, Griffiths, W., Finlay, K., Chakraborty, S., 2011. Climate change and diseases of food crops. Plant. Pathol. 60, 113–121.

Mahlein, A.K., Oerke, E.C., Steiner, U., Dehne, H.W., 2012. Recent advances in sensing plant diseases for precision crop protection. Eur. J. Plant Pathol. 133, 197–209.

Merton, R., 2007. Early Simulation Results Aries-1 Satellite Sensor Multi-Temporal Vegetation Research Derived Aviris.

Mika, S., Rätsch, G., Weston, J., Schölkopf, B., Müller, K.R., 1999. Fisher discriminant analysis with kernels, Neural Networks for Signal Processing Ix, 1999. In: Proceedings of the 1999 IEEE Signal Processing Society Workshop, pp. 41–48.

Mirik, M., Ansley Jr, R.J., G.J.M., Elliott, N.C., 2012. Spectral vegetation indices selected for quantifying Russian wheat aphid (Diuraphis noxia) feeding damage in wheat (Triticum aestivum L.). Precision Agric. 13, 501–516.

Moshou, D., Bravo, C., West, J., Wahlen, S., Mccartney, A., Ramon, H., 2004. Automatic detection of 'yellow rust' in wheat using reflectance measurements and neural networks. Comput. Electron. Agriculture 44, 173–188.

Pal, M., Foody, G.M., 2010. Feature selection for classification of hyperspectral data by SVM. Geosci. Remote Sens. IEEE Trans. 48, 2297–2307.

Penuelas, J., Baret, F., Filella, I., 1995. Semiempirical indexes to assess carotenoids chlorophyll-a ratio from leaf spectral reflectance. Photosynthetica 31, 221–230.

Penuelas, J., Gamon, J.A., Fredeen, A.L., Merino, J., Field, C.B., 1994. Reflectance indices associated with physiological changes in nitrogen- and water-limited sunflower leaves. Remote Sens. Environ. 48, 135–146.

Rumpf, T., Mahlein, A.K., Steiner, U., Oerke, E.C., Dehne, H.W., Mer, L., 2010. Early detection and classification of plant diseases with Support Vector Machines based on hyperspectral reflectance. Comput. Electron. Agriculture 74, 91–99.

Saadi, K., Talbot, N.L., Cawley, G.C., 2007. Optimally regularised kernel Fisher discriminant classification. Neural Networks Official J. Int. Neural Network Soc. 20, 832–841.

Savary, S., Ficke, A., Aubertot, J.N., Hollier, C., 2012. Crop losses due to diseases and their implications for global food production losses and food security. Food Security 4, 519–537.

Theodoridis, S., Koutroumbas, K., 2010. Pattern recognition 4th edition. J. Am. Water Resour. Assoc. 45, 22–34.

Van, G.T., Suykens, J.A., Lanckriet, G., Lambrechts, A., De, M.B., Vandewalle, J., 2002. Bayesian framework for least-squares support vector machine classifiers, gaussian processes, and kernel Fisher discriminant analysis. Neural Comput. 14, 1115–1147.

Yang, J., Jin, Z., Yang, J.Y., Zhang, D., Frangi, A.F., 2004. Essence of kernel Fisher discriminant: KPCA plus LDA. Pattern Recogn. 37, 2097–2100.

Yuan, L., Zhang, J., Zhao, J., Huang, W., Wang, J., 2013. Differentiation of yellow rust and powdery mildew in winter wheat and retrieving of disease severity based on leaf level spectral analysis. Spectroscope Spectral Anal. 33, 1608–1614 (1607).